SLAC-PUB-7190
June 1996

Neutron Fluence and Energy Spectra Around the Varian Clinac 2100C/2300C Medical Accelerator

K. R. Kase, X. S. Mao, W. R. Nelson, J. C. Liu

Stanford Linear Accelerator Center,
Stanford University, Stanford, CA, 94309

J. H. Kleck

Varian Corporation, Palo Alto, CA 94304

and

M. Elsalim

Science Applications International Corporation
Santa Clara, CA 95054

(Submitted to Health Physics Society)

Work supported by Department of Energy contract DE–AC03–76SF00515.

SLAC-Pub-7190

Neutron Fluence and Energy Spectra Around the Varian Clinac 2100C/2300C Medical Accelerator

K. R. KASE1[1], X. S. MAO[1], W. R. NELSON[1], J. C. LIU[1],

J. H. KLECK[2] AND M. ELSALIM[3]

ABSTRACT

We have simulated the head geometry of a Varian Clinac 2100C/2300C medical accelerator in a Monte Carlo calculation to produce photoneutrons and transport them through the head shielding into a typical therapy room (modeled by a test cell at Varian Associates). The fast neutron leakage fluence and energy spectra have been calculated at 7 positions around the linac head for typical beam operation at 10, 15, 18 and 20 MV. The results of these calculations have been compared with limited measurements made using the same model accelerator operating in a Varian test cell. Calculations were also made for the fluence and energy spectra outside the head with no surrounding concrete walls, floor or ceiling to eliminate the effects of scattering from concrete. Comparisons were also made with calculations using a much simplified head geometry. The results indicate that the calculations using the complex head geometry compare, within the uncertainties, with the measurements. The simple head geometry leads to differences of a factor of 2 from the complex geometry. Results of these calculations can be used to calculate fast neutron transmission through various shielding configurations and through labyrinths.

[1] Stanford Linear Accelerator Center, Stanford, CA 94309
[2] Varian corp., Palo Alto, CA 94304
[3] Science Applications International Corp., Santa Clara, CA 95054

INTRODUCTION

Electron linear accelerators (Linac) used for medical radiation therapy produce bremsstrahlung spectra in the energy range from 4 to 25 MV. Electrons and photons with energies above about 8 MeV can produce neutrons through direct electro-production or through the photonuclear giant dipole resonance reaction. These reactions occur in the various materials in the Linac target, flattening filter and collimation system, as well as in the patient. This neutron production has been discussed in general (NCRP 1984). Ing, et al. (1982), Nath, et al. (1984) and Agosteo, et al. (1993b) have studied the effect of these unwanted neutrons on the radiation dose to patients. Others (Uwamino, et al. 1986; Sanchez, et al. 1989; Tosi, et al. 1991; Agosteo, et al. 1995) have measured neutron energy spectra, fluence, or dose equivalent in treatment rooms. Comparisons of these measurements have been made with calculations using discrete ordinates transport of the measured spectrum (Uwamino, et al. 1986); using Monte Carlo transport of a calculated spectrum through a modeled accelerator head (Sanchez, et al. 1989); and using Monte Carlo transport of neutrons in a treatment room from a point source through a spherical tungsten shield (Agosteo, et al. 1995). LaRiviere (1985) measured the average energies of leakage neutrons at various positions in a treatment room and McKinley (1992) studied the neutron production when the primary photon beam was directed at metal or concrete slabs. Two papers by Agosteo, et al. (1993a, 1994) discuss calculation methods for estimating the leakage neutron fluence and are directed at developing an analytical method that produces results comparable with a Monte Carlo calculation. The neutron source spectrum was calculated analytically and the accelerator head geometry was a simple spherical tungsten shield surrounding a target. The calculation of photoneutron production in various targets has been presented in a recent paper by Mao, et al. (1996) and the production of neutrons in

the Varian Clinac 2100C/2300C is discussed in Mao, et al. (1997). In the latter publication the accelerator head was modeled precisely in a Monte Carlo code.

The investigation reported in this paper continues the previous work (Mao, et al. 1997) to determine the leakage neutron fluence and energy spectrum in a treatment room, outside the accelerator head. This information is relevant for determining the potential dose to a patient from these unwanted neutrons. It is also relevant for calculating shielding, and entrance labyrinth and duct designs for radiation protection. The methods for estimating leakage neutron fluence and energy that are given in NCRP Report No. 79 (1984) were very good for its time. However, they relied on a crude analytical formula to determine the neutron source, and simple measurements to determine the neutron fluence and average energy in the treatment room. That simple method requires verification, which is possible by using sophisticated Monte Carlo calculations. The effect of the complexity of the accelerator head design and the materials that are used needs further investigation.

We have used the EGS4 Monte Carlo code (Nelson et al. 1985) to calculate the neutron production in the Varian Clinac operating in the modes to produce x rays at 10, 15, 18 and 20 MV. This code was coupled with a modified version of the MORSE code (Emmett 1984) that incorporates the code EVAP4 (ORNL 1974) to calculate the neutron energy spectrum and to transport the neutrons (Liu, et al. 1997). The methods for calculating the locations and the magnitudes of the neutron sources for the Varian Clinac have been described (Mao et al. 1997).

In the work reported here we have used the methods described in the previous work to specify the fast neutron source terms and have transported the neutrons through the material comprising the accclerator head. We report the fast neutron fluence and energy spectra in the treatment room taking into account the scattering in concrete walls, ceiling and floor. Calculated results were compared, where possible with measurements that were made of the leakage epithermal neutrons from an

identical accelerator operated in the Varian test cells that were modeled for the calculations (Elsalim 1994). In these measurements, neutron fluences were measured using activation foils contained in cadmium-covered moderators and the neutron energy spectra were measured using Bonner spheres (Bramblett, et al. 1960). Average energies of the leakage neutrons were calculated from the measured spectra. These comparisons can serve to validate the Monte Carlo simulation and calculation. The techniques can then be applied with confidence for other accelerator designs. Comparisons of the calculations presented here with other previous work have little relevance because those results were presented as dose equivalent with no spectral information (Sanchez, et al. 1989), at different points relative to the source (Uwamino, et al. 1986), or both (Agosteo, et al. 1995).

Also, we have determined the neutron fluence, energy and angular distribution in the absence of a room. This information is useful as source terms for subsequent calculations of neutron transport through various configurations of shielding. An understanding of the transport and attenuation of neutrons produced by medical linacs is important for shielding design when high atomic number materials such as iron and lead are used in the room shielding. Knowledge of the source terms and energies of the neutrons is also important when studying the transport of radiation through the entrance labyrinths and ventilation ducts.

Finally, detailed calculations employing the complex geometry and material configuration of the Varian Clinac were compared with calculations employing a much simplified model of an accelerator target, filter, collimators and head shield. This comparison was made to determine if a generalized simple geometry would yield results that were similar to those calculated using the complex geometry. This is important because it would indicate if the neutron fluences and energies calculated using the Varian Clinac and reported here would be applicable to any medical accelerator operating

at similar energies regardless of manufacturer, e.g. comparisons with Uwamino, et al. (1986), Sanchez, et al. (1989), Tosi, et al. (1991) and Agosteo, et al. (1995).

The purpose of this report is to present a method for determining leakage fast neutron fluence and energy spectra that can be used for calculating dose to patients, and shielding and labyrinth designs. It also presents the results for a particular medical accelerator design and shows that it is difficult to generalize to a simplified or different head shielding configuration, similar to that used by Ing, et al. (1984) and Agosteo, et al. (1995), if the results are needed to better than a factor of 2.

METHODS

Details of the calculations for giant dipole resonance photoneutron and electro-production yield were described by Mao et al. (1996). The description of the simulation of a medical accelerator head using combinatorial geometry (Fig. 1) and the calculation of neutron yields in the Varian Clinac 2100C/2300C has also been published (Mao et al. 1997). The processes are summarized in the flow diagrams shown in Fig. 2. The EGS4 code is used to calculate the production and transport of photons that result from electrons impinging on the accelerator target. This creates a data file that specifies the photon position (x,y,z), direction (u,v,w), energy ($E\gamma$) and track length (l). The photon data can be used in EGS4 to convolute the track length and the photonuclear cross sections to calculate the neutron yield. However, to determine the photoneutron energy spectra, the photon data file is provided as input for subsequent calculations using the MORSE code. Neutrons are produced either through the direct process or the evaporation process. MORSE creates photoneutrons with the position (x,y,z), direction (u',v',w'), energy (En) and yield (Y_1, Y_2) from each photon in the data file (Liu et al. 1997). Following this MORSE is used to transport the neutrons through the accelerator head into the room, and to determine the neutron fluence and energy including their interactions with the concrete walls, ceiling and floor of the room.

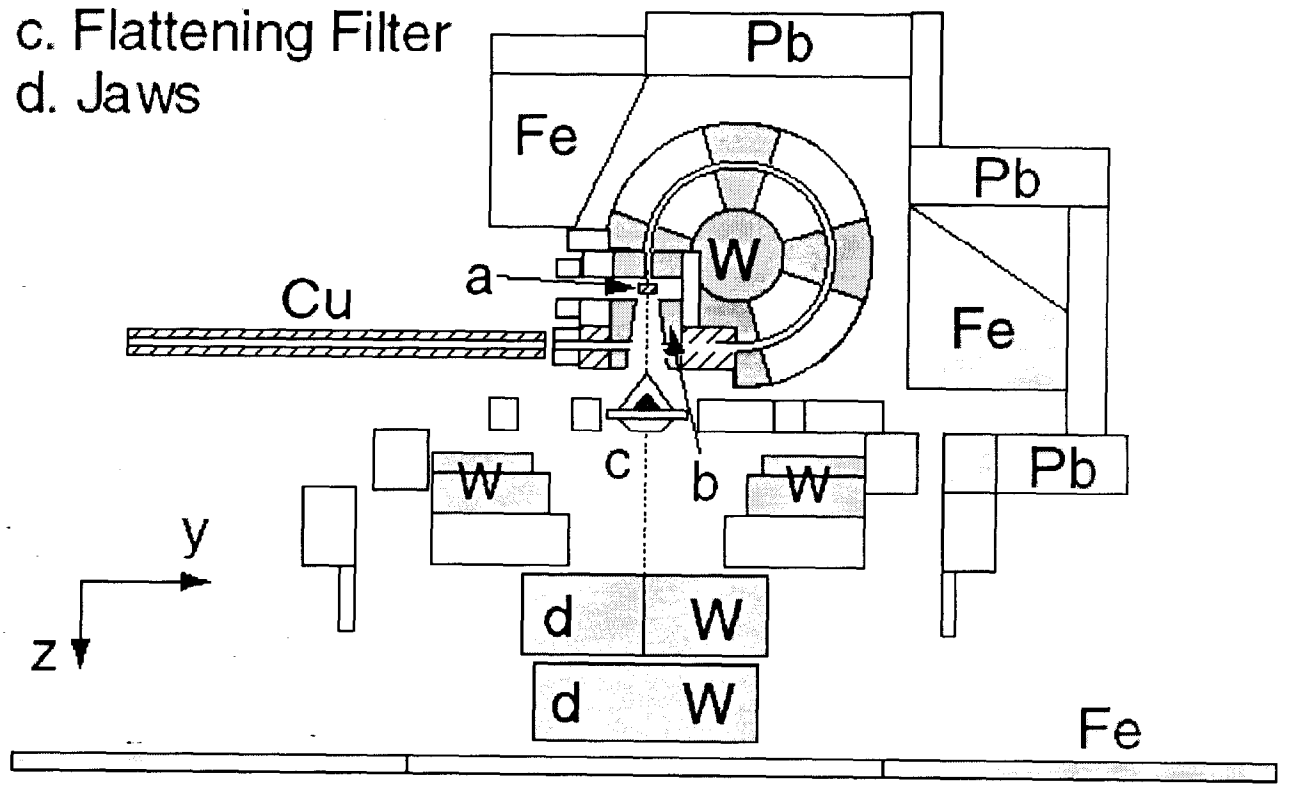

1. Fully-described geometry for computer simulation of accelerator head. a. Target; b. Primary Collimator; c. Flattening Filter; d. Variable Jaws.

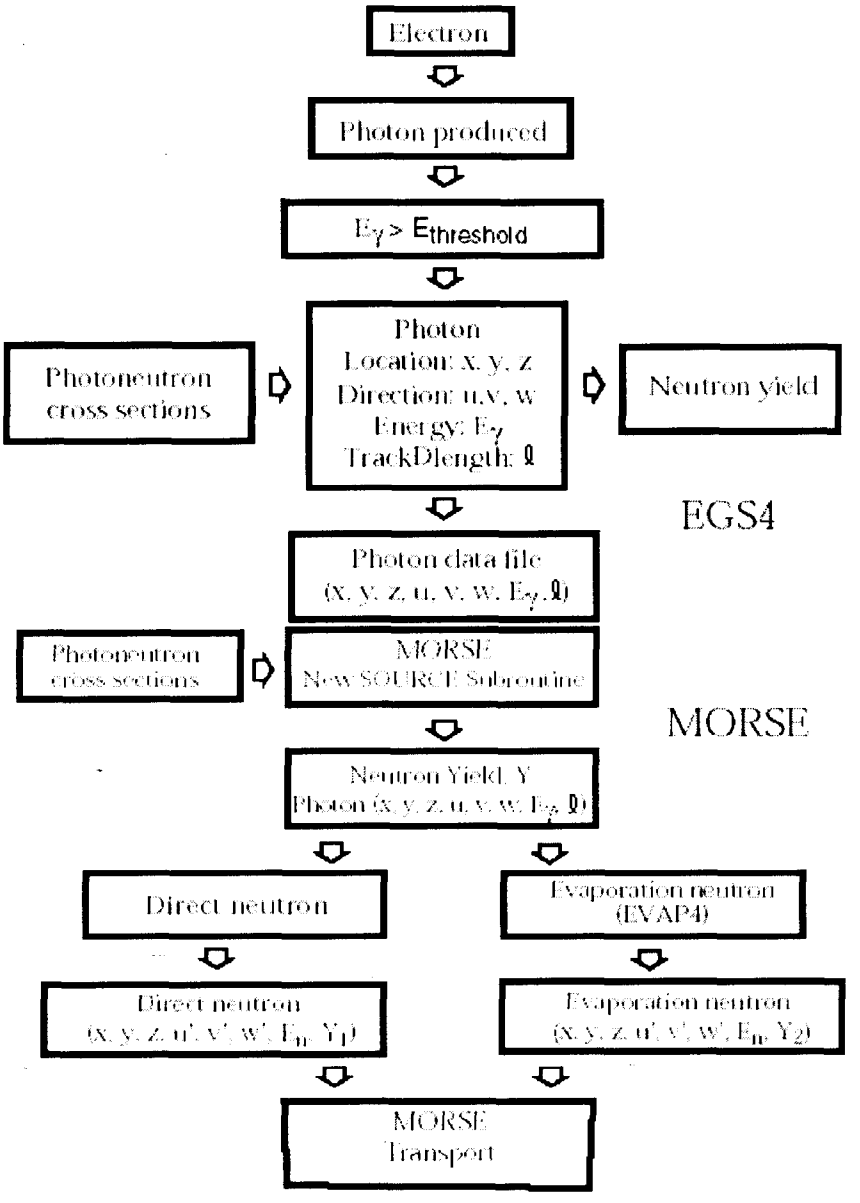

2. Flow chart of neutron yield and transport calculation using the EGS4 and MORSE codes.

The fully-described 85 body geometry was used in this calculation. Fig. 1 gives a two-dimensional representation of that geometry. Because of the complexity of the geometric representation of the accelerator head it is not practical to illustrate it in all its detail, including dimensions and materials. Consequently, we have provided the combinatorial geometry input data

for the EGS4 code in the Appendix. With minor modifications the input data can also be used with MORSE code.

For the 10.3 and 22.3 MeV electron energies two independent calculations were made using different random numbers to start both the EGS4 and the MORSE calculations. In each calculation enough electrons were directed onto the target to create a data file containing 10,000 photons. MORSE randomly sampled sufficient photons from the data file supplied to generate 7,500 source neutrons. At electron energies of 14.9 and 18.8 MeV five independent calculations were made at each energy, sampling sufficient photons to generate 15,000 source neutrons. The results at each energy were combined to determine the random error associated with the calculation.

The dimensions of the room were about 6.5 m x 7.0 m x 5 m and the concrete thickness was 0.6 m. The target was approximately centered in the room. The room size and target position were chosen to compare with measurements. Calculations were made, with the variable collimators closed, of the neutron fluence and energy spectra at 7 positions around the accelerator as shown in Fig. 3. The points were chosen to represent three locations in the plane of the patient (1, 2 & 7), and three points in the target plane (3, 5 & 6) and one point in the backward direction (4) that are important for shielding the leakage radiation. Points 5 and 6 would be expected to be symmetrical and have identical particle fluences if the internal shielding of the accelerator is symmetrical.

Measurements were made of neutron fluences and energies from Clinac 2100C/2300C, with collimators closed, in concrete test cells at Varian Associates. A Bonner sphere spectrometer was used (Bramblett et al. 1960). The measurement technique and the results of the measurements are described elsewhere (Elsalim 1994). Results of these measurements were compared at 3 or 4 positions around the Clinac head (Fig. 3) with the results of the calculations described above. To make the comparison the fluence per incident electron, determined from the calculation, was

converted to fluence per photon dose (Gy) at isocenter using the method described by Mao, et al. (1997).

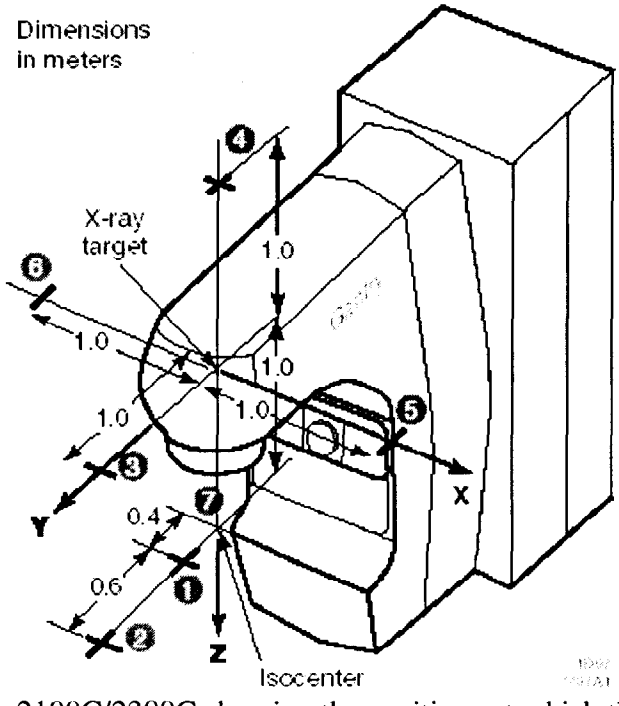

3. Diagram of Clinac 2100C/2300C showing the positions at which the neutron fluence and energy calculations and measurements were specified. Coordinates of points relative to the target (cm):

Position	x	y	z
1	0	40	100
2	0	100	100
3	0	100	0
4	0	0	-100
5	100	0	0
6	-100	0	0
7	0	0	100

Calculations were also made of the neutron fluence and energy spectra around the accelerator without the surrounding concrete walls, ceiling and floor. This was done to produce a set of data that can be used for subsequent studies of the transmission of the "leakage" neutrons through various configurations of shielding.

Finally, a set of calculations were made for the transmission of the neutrons through a simplified accelerator head geometry shown in Fig. 4. These calculations were done without the surrounding

concrete and were meant to determine to what extent the neutron fluence and energy are influenced by the materials and geometry of the accelerator head. If the results were similar for the two geometries (Figs. 1 & 4), they could be assumed to be similar for any other manufacturer's accelerator. This would simplify subsequent analyses of neutron dose and transmission.

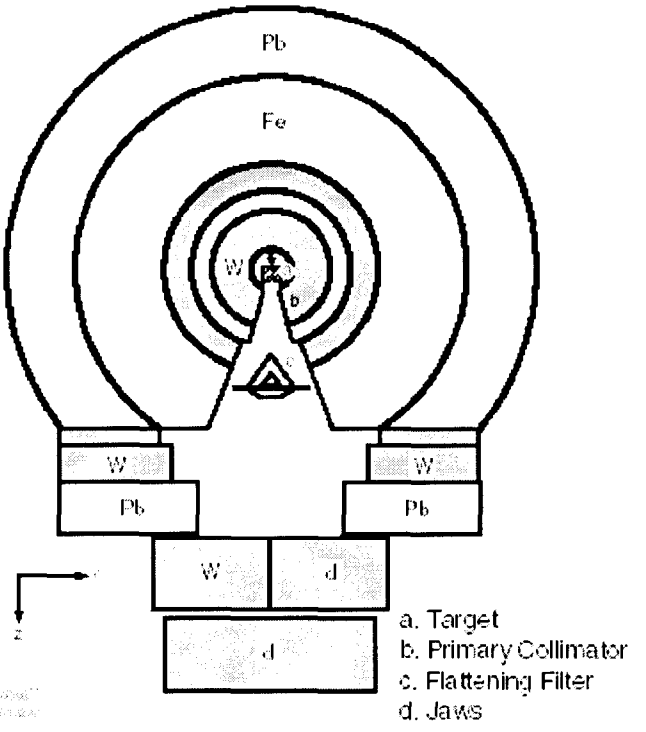

4.Simple geometry for computer simulation of accelerator head.

RESULTS

Calculations and measurements were made for incident electrons with nominal energies of 10, 15, 18 and 20 MV. The actual electron kinetic energies that were used in the calculations were 10.3, 14.9, 18.8 and 22.3 MeV corresponding with measurements of the electron kinetic energy at the target for the nominal energies stated. Total neutron yields for these energies were reported previously (Mao et al. 1997). The yields range from 3.8 x 10^{10} Gy^{-1} at 10 MV to 1.2 x 10^{12} Gy^{-1} at 18 and 20 MV normalized to photon dose at isocenter.

The fundamental measurable quantity, neutron fluence, was calculated for 7 positions and measured at 3 or 4 positions in the room around a Varian Clinac 2100C/2300C. Results are given in Table 1. Average energy is a quantity that is used in the recommended methods for calculating transmission of neutrons through shields and for calculating dose equivalent (NCRP 1984). The mean calculated and measured energies of the leakage neutrons are given in Table 2. Representative measured and calculated neutron energy spectra are shown in Figs. 5 and 6. The uncertainties in the fluence measurements are estimated to be ±15% (Elsalim 1994); uncertainty in the estimate of average energy is undoubtedly larger. The statistical uncertainties in the calculations depend upon the number of particle histories that were followed to determine the results. In this case these uncertainties are estimated to be ±15% at 20 MV, ±9% at 18 MV, ±7% at 15 MV and ±7% at 10 MV. The estimated systematic uncertainty caused by uncertainties in the photoneutron cross sections is less than ±20%, making the overall uncertainty in the calculated results of both fluence and energy in the range from ±25% to ±35%.

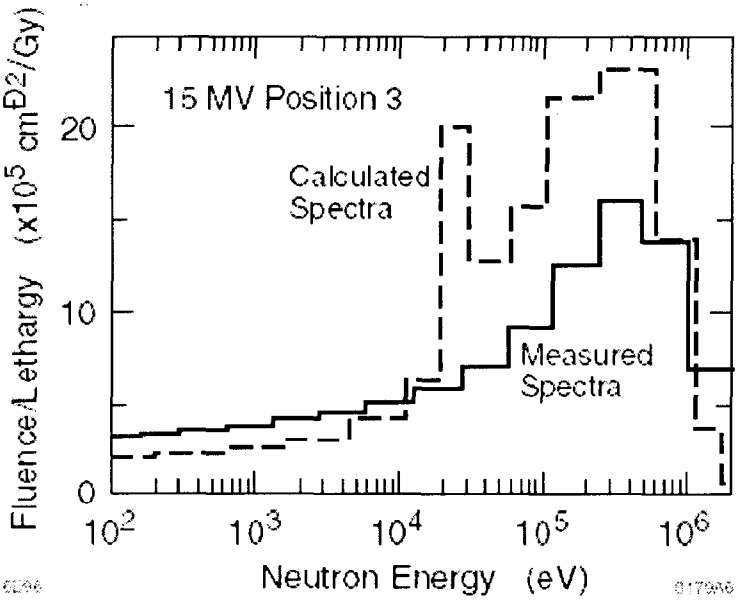

5.Calculated and measured neutron energy spectra for 14.9 MeV electron beam at position 3.

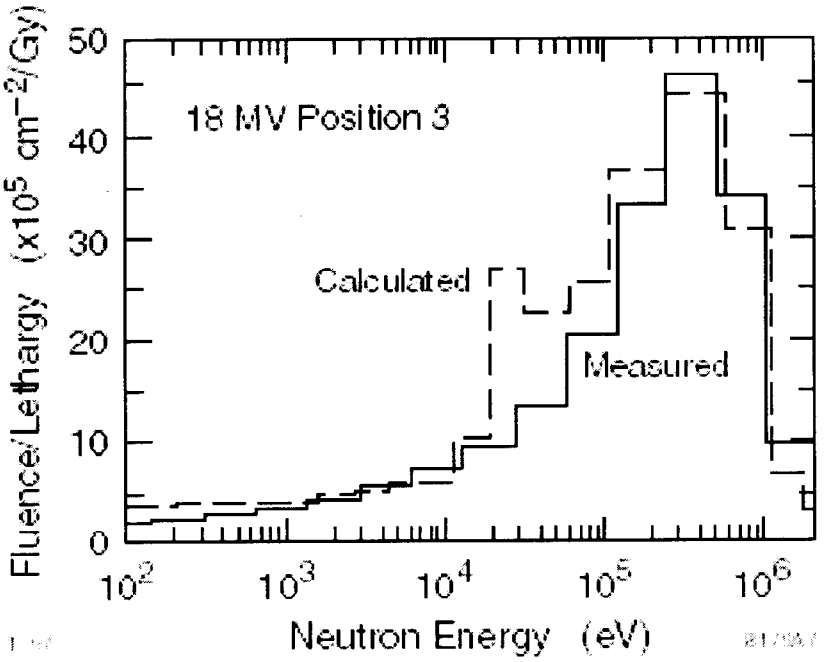

6. Calculated and measured neutron energy spectra for 18.8 MeV electron beam at position 3.

Table 1 Neutron Fluence in Concrete Room

	10	MV	15	MV	18	MV	20	MV
Position	Calculation 10^5 cm^{-2} Gy^{-1}	Measurement 10^5 cm^{-2} Gy^{-1}	Calculation 10^6 cm^{-2} Gy^{-1}	Measurement 10^6 cm^{-2} Gy^{-1}	Calculation 10^7 cm^{-2} Gy^{-1}	Measurement 10^7 cm^{-2} Gy^{-1}	Calculation 10^7 cm^{-2} Gy^{-1}	Measurement 10^7 cm^{-2} Gy^{-1}
1	3.5 ± 0.9	2.4 ± 0.4	7.6 ± 2.0	5.3 ± 0.8	1.4 ± 0.4	0.8 ± 0.1	1.5 ± 0.5	1.1 ± 0.2
2	1.6 ± 0.4	1.6 ± 0.2	3.7 ± 1.0	3.0 ± 0.5	0.7 ± 0.2	0.6 ± 0.1	0.7 ± 0.3	0.8 ± 0.1
3	1.8 ± 0.5	2.1 ± 0.3	4.3 ± 1.2	4.1 ± 0.6	0.8 ± 0.2	0.6 ± 0.1	0.9 ± 0.3	1.0 ± 0.2
4	1.5 ± 0.4		4.4 ± 1.2	5.0 ± 0.8	0.8 ± 0.2		0.9 ± 0.3	
5	3.0 ± 0.8		8.2 ± 2.2		1.5 ± 0.4		1.6 ± 0.6	

Table 2 Average Neutron Energy in Concrete Room

	10	MV	15	MV	18	MV	20	MV
Position	Calculation MeV	Measurement MeV	Calculation MeV	Measurement MeV	Calculation MeV	Measurement MeV	Calculation MeV	Measurement MeV
1	0.13	0.28	0.30	0.19	0.36	0.42	0.36	0.29
2	0.11	0.04	0.26	0.37	0.31	0.45	0.30	0.19
3	0.11	0.19	0.24	0.27	0.29	0.30	0.28	0.35
4	0.11		0.23	0.25	0.31		0.37	
5	0.14		0.34		0.43		0.47	
6	0.15		0.35		0.41		0.49	
7	0.13		0.26		0.31		0.34	

The results of the calculations without the surrounding concrete for both the complex and simplified geometries are given in Tables 3 and 4.

Table 3 Neutron Fluence Outside Head (no Concrete)

	10 MV		15 MV		18 MV		20 MV	
Position	Complex 10^5 cm^{-2} Gy^{-1}	Simple 10^5 cm^{-2} Gy^{-1}	Complex 10^6 cm^{-2} Gy^{-1}	Simple 10^6 cm^{-2} Gy^{-1}	Complex 10^7 cm^{-2} Gy^{-1}	Simple 10^7 cm^{-2} Gy^{-1}	Complex 10^7 cm^{-2} Gy^{-1}	Simple 10^7 cm^{-2} Gy^{-1}
1	3.0	1.7	5.4	4.2	1.1	0.7	1.2	0.7
2	0.9	1.2	1.9	3.1	0.3	0.5	0.4	0.5
3	1.2	1.6	2.5	5.0	0.5	0.8	0.5	0.9
4	0.8	0.5	2.1	2.0	0.5	0.4	0.5	0.4
5	2.4	1.7	6.0	4.9	1.2	0.8	1.2	0.9
6	2.4	1.7	5.9	5.0	1.2	0.9	1.3	0.9
7	3.5	1.4	6.1	3.2	1.2	0.5	1.4	0.6

Table 4 Neutron Average Energy Outside Head (no Concrete)

	10 MV		15 MV		18 MV		20 MV	
Position	Complex MeV	Simple MeV	Complex MeV	Simple MeV	Complex MeV	Simple MeV	Complex MeV	Simple MeV
1	0.16	0.16	0.39	0.37	0.43	0.43	0.47	0.43
2	0.17	0.16	0.42	0.36	0.46	0.43	0.49	0.44
3	0.14	0.15	0.35	0.33	0.38	0.39	0.40	0.42
4	0.16	0.12	0.32	0.26	0.47	0.34	0.46	0.35
5	0.17	0.15	0.39	0.36	0.48	0.39	0.58	0.40
6	0.17	0.16	0.41	0.32	0.50	0.39	0.57	0.40
7	0.15	0.16	0.33	0.35	0.38	0.39	0.40	0.41

DISCUSSION

As demonstrated previously the photoneutron yields calculated using the EGS4 code agreed with measurements within ±30% (Mao et al., 1997). This work shows that the fast neutron fluence determined by transport calculations through the head shielding of a typical medical linac generally compares with measurements of the fluence using identical accelerators and room geometries, within

the estimated uncertainties of both calculation and measurement. The agreement between calculated energy spectra and average energy is not as good. However, the uncertainty in measured energy spectra using Bonner spheres was not estimated (Elsalim 1994), and is probably large. We believe that calculations of the type described here using the current cross section data for photoneutron production and neutron interactions can be used to extend limited measurement information. The resulting uncertainties are of the order of ±30%.

Comparisons between the results of the fully-described geometry (Fig. 1) and the simplified geometry (Fig. 4) show that the simplified geometry as currently described is not adequate to determine the neutron fluence and energy distribution in the room to better than a factor of two. This is undoubtedly the result of the differences between the two models in their three-dimensional geometries. Consequently, it is not possible at this time to state that the results presented here can be generalized to all medical linear accelerators regardless of manufacturer. Further investigation is required.

The neutron data file that results from the calculations without the surrounding concrete room can be used as input for subsequent neutron transport calculations to determine the effectiveness of various room shielding configurations. This detailed study is the subject of a future report and may demonstrate that the shielding requirements are only slightly dependent upon the differences in the neutron fluence and energy distribution in the room. If so, the shielding requirements may be relatively independent of the linac manufacturer. This would be of considerable advantage in simplifying the design of shielding for medical linac facilities.

Results show that the neutron fluence at 1 meter from the target in a typical room varies by a factor of 2 to 3 when the collimators are closed. The variation in average energy is less than a factor of 2. For the Varian Clinac 2100C/2300C the fluence and average energy are highest in the patient plane

and lateral to the target. The variation in fluence appears to be slightly greater when the effects of scattering in the concrete are removed. The fluence is higher by a factor of about 50 at 20 MV when compared with that at 10 MV.

Measurements of the neutron energy spectrum are difficult and the results are more variable than the results obtained from the calculations. Because of the bin structure, the calculated energy spectra show a sharp peak at the Fe resonance energy of 0.023 MeV as would be expected when iron or steel is a major component of the head shielding configuration. The bin structure of the measured spectra unfolding calculations is such that this peak is not apparent. Average neutron energies following penetration of the head shield increase with initial electron energy from about 0.10 to 0.15 MeV for 10.3 MeV electrons to about 0.4 to 0.5 MeV for 22.3 MeV electrons. These values might be compared with the value of 0.25 MeV that is recommended in NCRP Report No. 79 (1984).

This work was supported by Department of Energy contract DE-AC03-76F00515

REFERENCES

Agosteo, S.; Froglio Para, A.; Maggioni, B. Neutron fluxes in therapy rooms. Med. Phys. 20:407-414; 1993a.

Agosteo, S.; Froglio Para, A.; Gerardi, F.; Silari, M.; Torresin, A.; Tosi, G. Photoneutron dose in soft tissue phantoms irradiated by 25 MV x-rays. Phys. Med. Biol. 38:1509-1528; 1993b.

Agosteo, S.; Froglio Para, A. Energy and spatial dependence of neutron fluxes in radiotherapy rooms for a simple dose estimate method. Nucl. Inst. Meth., Phys. Res. B 93:362-369; 1994.

Agosteo, S.; Froglio Para, A.; Maggioni, B.; Sangiust, V.; Terrani, S.; Borasi, G. Radiation transport in a radiotherapy room. Health Phys. 68:27-34; 1995.

Bramblett, R. L.; Ewing, R. J.; Bonner, T. W. A new type of neutron spectrometer. Nucl. Inst. Meth. 9:1-12; 1960.

Elsalim, M. M. Characterization of the neutron environment around Varian medical electron accelerators. Thesis, San Jose State University, San Jose, CA; 1994.

Emmett, M. B. The MORSE Monte Carlo radiation transport code system. ORNL-4972. Oak Ridge National Laboratory; 1984.

Ing, H.; Nelson. W. R.; Shore, R. A. Unwanted photon and neutron radiation resulting from collimated photon beams interacting with the body of radiotherapy patients. Med. Phys. 9:27-33; 1982.

LaRiviere, P. D. Neutron energies in medical electron accelerator rooms. Med. Phys. 12:769-775; 1985.

Liu, J. C.; Nelson, W. R.; Kase, K. R.; Mao, X. S. Calculations of the giant-dipole-resonance photoneutrons using a coupled EGS4-MORSE code. Radiat. Prot. Dosim. (Accepted for publication); 1997.

Mao, X.; Kase, K. R.; Nelson, W. R. Giant dipole resonance neutron yields produced by electrons as a function of target material and thickness. Health Phys. 70:207-214; 1996.

Mao, X.; Kase, K. R.; Liu, J. C.; Nelson, W. R.; Kleck, J. H.; Johnsen, S. Neutron sources in the Varian Clinac 2100C/2300C medical accelerator calculated by monte carlo. Health Phys. 72:523-528; 1997.

McGinley, P. H. Photoneutron fields in medical accelerator rooms with primary barriers constructed of concrete and metals. Health Phys. 63:678-701;1992.

Nath, R.; Epp, E. R.; Laughlin, J. S.; Swanson. W. P.; Bond, V. P. Neutrons from high-energy x-ray medical accelerators: An estimate of risk to the radiotherapy patient. Med. Phys. 11:231-241; 1984.

National Council on Radiation Protection and Measurements. Neutron Contamination form Medical Electron Accelerators, Report No. 79. National Council on Radiation Protection and measurements, Bethesda, MD; 1984.

Nelson, W. R.; Hirayama, H.; Rogers, D. W. O. The EGS4 code system. SLAC-265. Stanford Linear Accelerator Center; 1985.

ORNL. The EVAP calculation of particle evaporation from excited compound nuclei. PSR-10. Oak Ridge National Laboratory; 1974.

Sanchez, F.; Madurga, G.; Arrans, R. Neutron measurements around an 18 MV linac. Radiotherapy and Oncology 15:259-265; 1989.

Tosi, G.; Torresin, A.; Agosteo, S.; Foglio Para, A.; Sangiust, V.; Zeni, L; Silari, M. Neutron measurements around medical electron accelerators by active and passive detection techniques. Med. Phys. 18:54-60; 1991

Uwamino, Y.; Nakamura, T.; Ohkubo, T.; Hara, A. Measurement and calculation of neutron leakage from a medical electron accelerator. Med. Phys. 13:374-384; 1986.

APPENDIX

1. Varian Accelerator head 20MV (Jaws closed)

```
******************************
Incident Particle Data cards
******************************
   22.3                              EKEIN (MeV)
    0.0     0.0     0.001      XI,YI,ZI
    0.0     0.0     1.0        UI,VI,ZI

******************************
Combinatorial Geometry cards
******************************
 RPP    1    -75.0      75.0      -75.0      75.0      -75.0      75.0
 RPP    2    -70.0      70.0      -70.0      70.0      -70.0      70.0
 RCC    3      0.0       0.0        0.0       0.0        0.0     0.0635    0.301
 RCC    4      0.0       0.0     0.0634       0.0        0.0      1.026    0.301
 RCC    5      0.0       0.0     -0.254       0.0        0.0       .524    0.889
 RCC    6      0.0       0.0     -0.254       0.0        0.0      1.524    0.301
 RPP    7   -4.445     4.445      -6.35     4.826       2.54      4.445
 RCC    8      0.0     -8.89      0.508       0.0      2.541        0.0     2.54
 RCC    9      0.0     -8.89      0.508       0.0     12.448        0.0     1.27
 RCC   10      0.0       0.0      -2.54       0.0        0.0      6.985    3.557
 RPP   11   -4.445     4.445      -6.35     8.509      4.444     7.9375
 RCC   12      0.0     -8.89       6.19       0.0      2.541        0.0      1.5
 RCC   13      0.0     -8.89       6.19       0.0     17.399        0.0    0.4445
 TRC   14      0.0       0.0      7.940       0.0        0.0     -6.338     2.16    0.578
 RCC   15      0.0       0.0      4.444       0.0        0.0     3.4935     2.54
 RCC   16      0.0       0.0      -2.55       0.0        0.0       1.80    0.302
 TRC   17      0.0       0.0     12.446       0.0        0.0     -3.294     2.54    0.002
 TRC   18      0.0       0.0     12.444       0.0        0.0     -1.410   1.3335    0.002
 RCC    1      0.0       0.0     12.445       0.0        0.0      0.152     3.81
 TRC   20      0.0       0.0     12.596       0.0        0.0      0.749     2.79    1.580
 RPP   21    -7.04      -4.5      -6.35    -0.635      -2.54     7.9375
 RPP   22     4.50      7.04      -6.35    -0.635      -2.54     7.9375
 RCC   23    -3.81      8.65      -2.54      7.62        0.0        0.0    4.445
 RCC   24    -3.81      8.65      -2.54      7.62        0.0        0.0    12.70
 RCC   25   -10.15      8.65      -2.54     +20.3        0.0        0.0    12.70
 WED   26    -3.81      -3.3      -6.86       0.0      5.967     -16.762
                0.0     11.95       4.32      7.62        0.0        0.0
 WED   27    -3.81      12.8     -14.55       0.0      17.02      5.588
                0.0     -4.15      12.01      7.62        0.0        0.0
 WED   28    -3.81     20.82       1.27       0.0     -6.096     17.018
```

		0.0	-12.17	-3.81	7.62	0.0	0.0	
RPP	2	-10.15	+10.15	+1.20	+8.509	+7.9375	+10.6375	
RPP	30	-10.159	+10.159	-15.494	-7.239	-19.812	-5.207	
WED	31	-10.159	-7.240	-19.812	0.0	+7.239	0.0	
		0.0	0.0	+14.605	+20.318	0.0	0.0	
RPP	32	-20.32	+20.32	+25.146	+40.386	+2.286	+9.906	
WED	33	-20.32	+25.146	+2.287	0.0	0.0	10.16	
		0.0	+15.24	0.0	+40.64	0.0	0.0	
RPP	34	-3.81	+3.81	-7.62	-4.32	-5.08	-2.55	
RPP	35	-20.32	-10.16	-15.494	+7.366	-19.812	-2.032	
RPP	36	+10.16	+20.32	-15.494	+7.366	-19.812	-2.032	
RPP	37	-20.32	-10.16	+7.360	+25.15	-19.812	+9.906	
RPP	38	+10.16	+20.32	+7.360	+25.15	-19.812	+9.906	
WED	39	+10.16	-15.494	-2.023	0.0	0.0	+3.547	
		+10.16	0.0	0.0	0.0	+22.86	0.0	
WED	40	-10.16	-15.494	-2.023	-10.16	0.0	0.0	
		0.0	0.0	+3.547	0.0	+22.86	0.0	
RPP	41	-20.32	+20.32	-15.494	0.0	-23.622	-19.820	
RPP	42	-20.32	+20.32	-0.01	+25.147	-26.162	-19.820	
RPP	43	-20.32	+20.32	+25.146	+27.686	-26.162	-11.67	
RPP	44	-20.32	+20.32	+25.146	+44.196	-11.68	-7.87	
RPP	45	-20.32	+20.32	+40.386	+44.196	-7.870	+14.224	
RPP	46	-7.62	+7.62	+33.34	+46.040	+14.225	+19.69	
RPP	47	-3.81	+3.81	-7.112	-4.572	+11.17	+13.71	
RPP	48	-3.81	3.81	+5.08	+22.86	+11.17	+13.71	
RCC	49	0.0	0.0	+11.174	0.0	0.0	2.54	+12.7
RCC	50	0.0	0.0	+11.174	0.0	0.0	2.54	+15.24
RCC	51	0.0	0.0	+16.510	0.0	0.0	+1.90	+11.43
RCC	52	0.0	0.0	+16.510	0.0	0.0	+1.90	+20.955
RCC	53	0.0	0.0	+18.414	0.0	0.0	3.81	+10.16
RCC	54	0.0	0.0	+18.414	0.0	0.0	3.81	+20.955
RCC	55	0.0	0.0	+22.230	0.0	0.0	5.075	+7.62
RCC	56	0.0	0.0	+22.230	0.0	0.0	5.075	+20.955
RPP	57	-9.398	+9.398	-11.938	0.0	+28.067	+35.687	
RPP	58	-9.398	+9.398	0.0	+11.938	+28.067	+35.687	
RPP	59	-13.462	0.0	-10.795	+10.795	+36.703	+44.323	
RPP	60	0.0	+13.462	-10.795	+10.795	+36.703	+44.323	
RCC	61	0.0	0.0	+19.68	0.0	0.0	7.62	+28.26
RCC	62	0.0	0.0	+19.69	0.0	0.0	7.62	+33.34
RCC	63	0.0	0.0	+27.31	0.0	0.0	6.35	+28.26
RCC	64	0.0	0.0	+27.31	0.0	0.0	6.35	+29.53
RCC	65	0.0	0.0	+14.0	0.0	0.0	5.69	+21.5
RCC	66	0.0	0.0	+14.0	0.0	0.0	5.69	+25.945
RPP	67	-24.394	-20.33	-25.654	+32.38	-12.7	+8.89	
RPP	68	+20.33	+24.394	-25.654	+32.38	-12.7	+8.89	
RPP	69	-10.15	-4.445	-4.06	+8.65	-2.54	+10.6375	

RPP	70	+4.445	+10.15	-4.06	+8.65	-2.54	+10.6375		
RCC	71	-0.3	+8.65	-2.54	+0.6	0.0	0.0	+8.43	
RCC	72	-0.3	+8.65	-2.54	+0.6	0.0	0.0	9.03	
RCC	73	0.0	-50.0	+6.19	0.0	+40.0	0.0	+0.5	
RCC	74	0.0	-50.0	+6.19	0.0	+40.0	0.0	+1.0	
WED	75	-9.398	-15.506	+35.687	0.0	0.0	-0.508		
		0.0	+3.408	0.0	+18.796	0.0	0.0		
WED	76	-9.398	+15.506	+35.687	0.0	-3.048	0.0		
		0.0	0.0	-0.508	+18.796	0.0	0.0		
WED	77	-17.894	-10.795	+44.323	+1.524	0.0	0.0		
		0.0	0.0	-7.620	0.0	+21.584	0.0		
WED	78	+17.894	-10.795	+44.323	0.0	0.0	-7.62		
		-1.524	0.0	0.0	0.0	+21.584	0.0		
RPP	79	-24.40	+24.40	+28.26	+33.33	+14.225	+19.680		
RPP	80	-29.49	-24.41	-25.654	+44.20	+6.985	+14.0		
RPP	81	+24.41	+29.49	-25.654	+44.20	+6.985	+14.0		
RPP	82	-28.175	-25.0	-13.97	+13.97	+35.0	+45.16		
RPP	83	+25.0	+28.175	-13.97	+13.97	+35.0	+45.16		
RCC	84	0.0	0.0	45.720	0.0	0.0	+1.905	+22.860	
RCC	85	0.0	0.0	45.720	0.0	0.0	+1.905	+60.960	

END

VacuumOR		+2	-7	-8	-11	-12	-17	-21	-22
		-25	-30	-31	-32	-33	-34	-35	-36
		-37	-38	-39	-40	-41	-42	-43	-44
		-45	-46	-48	-50	-79	-57	-58	-59
		-60	-62	-64	-66	-67	-68	-74	-80
		-81	-82	-83	-85OR	+49	-17	-19	-20
		-47	-48OR	+14OR	+16OR	+9	-5OR	+63	-57
		-58OR	+65	-52	-54OR	+13OR	+6	-3	-4
	OR	+69OR	+70OR	+72	-71	-11	-7OR	+61	-56
		-54OR	+75OR	+76OR	+77OR	+78OR	+73OR	+51OR	+53
	OR	+55OR	+29OR	+84					

Target1	+3								
Target2	OR	+4	-3OR	+5	-6				
Primary Collimator									
	OR	+10	-16	-9	-14OR	+15	-13	-14	
Other	OR	+7	-10	-9OR	+8	-9OR	+12	-13	
Othe	OR	+11	-13	-15OR	+74	-73			
Flattening filter									
		+18OR	+17	-18OR	+19OR	+20			
Other	OR	+25	-24	-7	-11	-29	-69	-70OR	+26
		+24	-23	+71OR	+26	+24	-23	-72OR	+27
		+24	-23	+71OR	+27	+24	-23	-72OR	+28
		+24	-23	+71OR	+28	+24	-23	-72	

Other	OR	+24	-23	-26	-27	-28	-29	-7	-11
		+71OR	+24	-23	-26	-27	-28	-29	-7
		-11	-72OR	+21OR	+22	+23	-7OR	+34	
Other	OR	+30OR	+31OR	+32OR	+33OR	+35OR	+36OR	+37OR	+38
	OR	+39OR	+40						
Other	OR	+41OR	+42OR	+43OR	+44OR	+67OR	+68		
Other	OR	+46OR	+47OR	+48OR	+50	-49			
Other	OR	+52	-51OR	+54	-53OR	+45			
Other	OR	+66	-65OR	+80OR	+81				
Other	OR	+56	-55OR	+62	-61OR	+64	-63OR	+79	
Jaws	OR	+57	-75OR	+58	-76OR	+59	-77OR	+60	-78
Other	OR	+82OR	+83OR	+85	-84				
Null	+1	-2							

END

****

MEDIUM-region cards (24A1)

****

W
CU
W
FE
CU
TA
FE
FE
W
PB
FE
PB
PB
W
FE
PB
W
FE

****

DISCARD-region cards (36I2)

****

0 0 0 0 0 0 0 0 0 0 0 0 0 0 0 0 0 0 0 0 0 0 0 0 0 0 0 0 0 0 0 0 0 0 0 0 1

2.Varian Accelerator head 18MV (Jaws closed)

(only list the difference from 20MV data)

****

Incident Particle Data cards

****
18.8 EKEIN (MeV (kinetic energy)
****
Combinatorial Geometry cards
****

TRC	17	0.0	0.0	12.446	0.0	0.0	-3.2311	2.794	0.002
TRC	18	0.0	0.0	12.444	0.0	0.0	-1.3335	1.3335	0.002
RCC	19	0.0	0.0	12.445	0.0	0.0	0.436	3.81	
TRC	20	0.0	0.0	12.88	0.0	0.0	0.67	2.39	1.427

3.Varian Accelerator head 15MeV (Jaws closed)
(only list the difference from 20MV data)
****
Incident Particle Data cards
****
14.9 EKEIN (MeV (kinetic energy)
****
Combinatorial Geometry cards
****

RCC	4	0.0	0.0	0.0634	0.0	0.0	0.802	0.301	
TRC	17	0.0	0.0	12.446	0.0	0.0	-1.814	2.63	0.001
TRC	18	0.0	0.0	12.444	0.0	0.0	-0.410	1.3335	0.002
RCC	19	0.0	0.0	12.445	0.0	0.0	0.037	3.81	
RCC	20	0.0	0.0	12.482	0.0	0.0	0.04	3.81	

****
MEDIUM-region cards (24A1)
****

W
CU
W
FE
CU
W
W
FE
W
PB
FE
PB
PB
W
FE

PB
W
FE

4.Varian Accelerator head 10MV (Jaws closed)
(only list the difference from 20MV data)

```
******************************
 Incident Particle Data cards
******************************
      10.3                                EKEIN   (MeV (kinetic energy)
******************************
 Combinatorial Geometry cards
******************************

RCC     3       0.0     0.0     0.0     0.0     0.0     0.008   0.301
RCC     4       0.0     0.0     0.007   0.0     0.0     0.501   0.301
TRC     17      0.0     0.0     12.446  0.0     0.0     -3.213  2.794   0.0635
RCC     19      0.0     0.0     12.445  0.0     0.0     0.2931  3.81
TRC     20      0.0     0.0     12.738  0.0     0.0     0.785   2.032   0.127

******************************
 MEDIUM-region cards (24A1)
******************************
```

CU
CU
W
FE
CU
CU
CU
FE
W
PB
FE
PB
PB
W
FE
PB
W
FE